Magnetic Resonance in Medicine 57:141–149 (2007)

Variance of Estimated DTI-Derived Parameters via First-Order Perturbation Methods

Lin-Ching Chang,* Cheng Guan Koay, Carlo Pierpaoli, and Peter J. Basser

In typical applications of diffusion tensor imaging (DTI), DT-derived quantities are used to make a diagnostic, therapeutic, or scientific determination. In such cases it is essential to characterize the variability of these tensor-derived quantities. Parametric and empirical methods have been proposed to estimate the variance of the estimated DT, and quantities derived from it. However, the former method cannot be generalized since a parametric distribution cannot be found for all DT-derived quantities. Although powerful empirical methods, such as the bootstrap, are available, they require oversampling of the diffusion-weighted imaging (DWI) data. Statistical perturbation methods represent a hybrid between parametric and empirical approaches, and can overcome the primary limitations of both methods. In this study we used a first-order perturbation method to obtain analytic expressions for the variance of DT-derived quantities, such as the trace, fractional anisotropy (FA), eigenvalues, and eigenvectors, for a given experimental design. We performed Monte Carlo (MC) simulations of DTI experiments to test and validate these formulae, and to determine their range of applicability for different experimental design parameters, including the signal-to-noise ratio (SNR), diffusion gradient sampling scheme, and number of DWI acquisitions. This information should be useful for designing DTI studies and assessing the quality of inferences drawn from them. Magn Reson Med 57:141–149, 2007. Published 2006 Wiley-Liss, Inc.†

Key words: DTI; variance; uncertainty; perturbation; error propagation

The number and scope of diffusion tensor imaging (DTI) applications have increased dramatically since this technique was first introduced. In a critical-care context, DTI can be used to provide maps of the average apparent diffusion coefficient (mean ADC) or trace-weighted images, which are both helpful for managing acute stroke (1). Other tensor-derived quantities, such as the fractional anisotropy (FA), are used to assess white matter (WM) involvement in chronic stroke (2), multiple sclerosis (3,4), and other neurodegenerative diseases (5). WM tracts visualized with the use of color-coded maps (6) or by following the direction of maximum diffusivity (7) are helpful for planning neurosurgical procedures (8) and inferring anatomical connectivity between different brain regions (9). Multicenter studies are now being undertaken that use DTI data to construct brain atlases of normal and abnormal human brains (10). Typically, each of these applications uses a particular set of DT-derived quantities to make a diagnostic, therapeutic, or scientific determination.

Each application of DTI also has an optimal or near-optimal experimental design. For instance, when estimating the mean ADC or trace of the DT in acute stroke, it is desirable to use the fewest possible diffusion-weighted (DW) images to minimize the acquisition time (11). In tractography it is prudent to acquire 30 or more DW images whose diffusion gradient orientations are isotropically arranged on a spherical shell (12). For a longitudinal study using DTI, a robust protocol with high reproducibility of DW imaging (DWI) data is desired. A multicenter prospective study using DTI requires an experimental design with high sensitivity and low interobserver variability. Characterizing the variability of tensor-derived quantities is critical to each application. Knowledge of this variability will help determine, among other things, whether using a scheme with more gradient directions or using repeated measurements along each gradient direction is desired for a multicenter study.

Several approaches have been proposed to estimate the variance of the DT itself, and quantities derived from it. Pajevic and Basser (13) showed that for a signal-to-noise ratio (SNR) greater than 5, and more than seven DWI acquisitions, a multivariate Gaussian distribution adequately describes the variability of the estimated DT. This parametric distribution was also used to derive the distribution of trace that is also normally distributed (14).

Pajevic and Basser (13) also showed that this multivariate Gaussian distribution could be recast as a normal distribution of a second-order tensor random variable. In certain circumstances, it can be used to predict the distribution of the eigenvalues of the estimated DT (assuming an unweighted linear model). However, to date it has not been possible to use it to derive the parametric distribution of other widely used tensor-derived quantities, such as the FA, relative anisotropy (RA), or eigenvectors of the DT.

Empirical statistical distributions have also been used to characterize variability in the DTI experiment. Pierpaoli et al. (15) used Monte Carlo (MC) methods to simulate the variability of ideal DTI data when only Gaussian noise is added to each RF channel in quadrature. Subsequently, Pajevic and Basser (13) showed that the bootstrap method could be used to estimate the distribution of the DT itself and of tensor-derived quantities from actual DTI data. Although such empirical methods are powerful, they require the acquisition of additional DW images, which is onerous for many biological and clinical applications.

Statistical perturbation methods contain elements of both parametric and empirical approaches (16–18). They allow errors in the DT to be propagated through to errors in the DT-derived quantities using the analytical expressions

Section on Tissue Biophysics and Biomimetics, Laboratory of Integrative Medicine and Biophysics, National Institute of Child Health and Human Development, National Institutes of Health, Bethesda, Maryland, USA.

Grant sponsor: National Institute of Child Health and Human Development (NICHD) Intramural Research Program.

*Correspondence to: Lin-Ching Chang, National Institutes of Health, Building 13, Room 3W16, 13 South Drive, Bethesda, MD 20892-5772. E-mail: changlin@nih.gov

Received 29 March 2006; revised 7 August 2006; accepted 13 September 2006.

DOI 10.1002/mrm.21111
Published online in Wiley InterScience (www.interscience.wiley.com).

relating them. Perturbation analysis overcomes the primary limitation of the parametric approaches described above, since analytic or approximate relationships can be established between the DTs and any of the aforementioned tensor-derived quantities. It also overcomes the primary limitation of empirical statistical approaches, such as the bootstrap, since no additional DW images are required for the particular experimental design to estimate the variance of a tensor-derived quantity.

First-order matrix perturbation analysis was first used in DTI to examine uncertainty in the eigenvalues and eigenvectors, with the goal of estimating the variance of the fiber orientation (16). Subsequently Anderson (17) proposed using second- and higher-order perturbations to determine the uncertainty in various quantities derived from the DT, such as its eigenvalues, eigenvectors, and trace.

Skare et al. (20) employed error propagation analysis to determine how noise in DWI data affects the uncertainty in the estimated ADCs (19) and in diffusion anisotropy measures. Another recent study used singular-value decomposition to determine the tensor variance and the error propagation method to derive the uncertainty in diffusion anisotropy measures such as FA and RA, but neglected the covariance terms between the DT elements in its formulae (18).

We used a first-order perturbation method to obtain estimates of the variance of the DT, eigenvalues, and eigenvectors, and the error propagation method to determine other tensor-derived quantities, such as the trace, FA, and RA, for a given experimental design. We performed MC simulations of DTI experiments to validate these formulae, and to determine their applicability over a broad range of experimental design parameters, including SNR, number of diffusion gradient directions, number of DWI acquisitions, etc. This information should be useful for designing DTI studies and assessing the quality of inferences drawn from DTI studies.

MATERIALS AND METHODS

Review of Log Linear Model Tensor Estimation

Let $\mathbf{y} = \{\ln(S_1), \ldots, \ln(S_N)\}^T$, where S_i represents the i^{th} DWI magnitude signal intensity in a DTI acquisition, and $\boldsymbol{\alpha} = \{D_{xx}, D_{yy}, D_{zz}, D_{xy}, D_{xz}, D_{yz}, \ln(A_0)\}^T$ are the DTI model parameters, where D_{ij} are elements of the DT, and A_0 is the echo intensity with no applied gradients (21). To first order, the log linear model can be written as $\boldsymbol{y} = \boldsymbol{B}\alpha + \boldsymbol{e}$, where the j^{th} row of $\boldsymbol{B}$ contains b-matrix entries of the j^{th} DWI acquisition $-\{b_{xxj}, b_{yyj}, b_{zzj}, 2b_{xyj}, 2b_{xzj}, 2b_{yzj}, -1\}$, and $\boldsymbol{e}$ is the error vector. The diagonal elements of the covariance matrix of $\boldsymbol{e}$ equal the signal variance divided by the signal intensity, i.e., $[\Sigma_{\boldsymbol{e}}]_{ii} = \sigma_i^2/\langle S_i\rangle^2$, where $\langle S_i\rangle$ denotes the expectation of random variable S_i, and σ_i^2 is the intensity variance. Measured $\mathbf{y}$ data are assumed to be independent, so the off-diagonal elements of the covariance matrix of $\boldsymbol{e}$ are zero, i.e., $[\Sigma_{\boldsymbol{e}}]_{ij} = 0$, where $i \neq j$. The weighted least-squares solution using the linear model is given by (21):

$$\alpha = (\boldsymbol{B}^T\tilde{\Sigma}_{\boldsymbol{e}}^{-1}\boldsymbol{B})^{-1}(\boldsymbol{B}^T\tilde{\Sigma}_{\boldsymbol{e}}^{-1})\boldsymbol{y} \quad [1]$$

where $\tilde{\Sigma}_{\boldsymbol{e}}$ is the diagonal matrix that can be obtained using the measured signal intensities and given noise variance, and matrix $\boldsymbol{B}$ is given by the experimental design (22).

Assuming that the estimation of the covariance matrix of the measured data is accurate (i.e., $\tilde{\Sigma}_{\boldsymbol{e}} \approx \Sigma_{\boldsymbol{e}}$), the covariance matrix of the estimated tensor will be given by

$$\Sigma_\alpha = \langle\alpha^T\rangle \approx (\boldsymbol{B}^T\tilde{\Sigma}_{\boldsymbol{e}}^{-1}\boldsymbol{B})^{-1}. \quad [2]$$

Matrix Perturbation and Error Propagation Theory

Let $\boldsymbol{D_0}$ be a real, symmetric 3×3 unperturbed DT matrix, and let $\Delta\boldsymbol{D}$ be a real, symmetric 3×3 perturbation matrix corresponding to it; then the estimated tensor, $\boldsymbol{D} = \boldsymbol{D_0} + \Delta\boldsymbol{D}$. Using first-order matrix perturbation analysis (16,23,24), one can estimate the variance of three eigenvalues and eigenvectors of DTs directly from the estimated tensor $\boldsymbol{D}$ using Eq. [1] and its estimated perturbation matrix $\Delta\boldsymbol{D}$, which contains the standard errors of each component of $\boldsymbol{D}$ using Eq. [2]. Similarly to expressions shown by Anderson (17), the mean square diagonal elements of $\Delta\boldsymbol{D}$ are $[\Delta\boldsymbol{D}]_{ii}^2 = \langle(\boldsymbol{D} - \boldsymbol{D_0})_{ii}^2\rangle = [\boldsymbol{\Sigma}_\alpha]_{ii}$ (i < 3). To be more specific, we can write $\sigma_{xxxx}^2 = [\Delta\boldsymbol{D}]_{00}^2 = [\Sigma_\alpha]_{00}$, $\sigma_{yyyy}^2 = [\Delta\boldsymbol{D}]_{11}^2 = [\Sigma_\alpha]_{11}$, $\sigma_{zzzz}^2 = [\Delta\boldsymbol{D}]_{22}^2 = [\Sigma_\alpha]_{22}$. The covariance terms of tensor elements can be computed using $\sigma_{xxyy}^2 = \sigma_{yyxx}^2 = [\Delta\boldsymbol{D}]_{01}^2 = [\Sigma_\alpha]_{01}$, $\sigma_{xxzz}^2 = \sigma_{zzxx}^2 = [\Delta\boldsymbol{D}]_{02}^2 = [\Sigma_\alpha]_{02}$, and $\sigma_{yyzz}^2 = \sigma_{zzyy}^2 = [\Delta\boldsymbol{D}]_{12}^2 = [\Sigma_\alpha]_{12}$. Note that if the signal variance is assumed to be a constant in the image, one can write $\Sigma_\alpha = \tilde{\Sigma}_{\boldsymbol{e}}(\boldsymbol{B}^T\boldsymbol{B})^{-1}$ and derive the relationship between the variance of each tensor element and the squared SNR, which can be defined as $\langle S_i\rangle^2/\sigma^2$.

Let λ_i be the i^{th} eigenvalue and $\boldsymbol{\epsilon}_i$ be its corresponding eigenvector. Let the uncertainty of λ_i be $\Delta\lambda_i$ and the uncertainty of $\boldsymbol{\epsilon}_i$ be $\Delta\boldsymbol{\epsilon}_i$. One can compute the uncertainty for each eigenvalue, $\sigma_{\lambda_i}^2$, using the first-order correction (23,24) (see also Appendix A for a brief description):

$$\sigma_{\lambda_i}^2 = \langle\Delta\lambda_i^2\rangle = \langle(\varepsilon_i^T\Delta\boldsymbol{D}\varepsilon_i)^2\rangle. \quad [3]$$

If we assume that the three sorted eigenvalues of $\boldsymbol{D_0}$ have $\lambda_1 > \lambda_2$ and $\lambda_1 > \lambda_3$, it can also be shown that the perturbation of the eigenvector associated with the largest eigenvalue is given by

$$\Delta\varepsilon_1 = \left(\frac{\varepsilon_1^T\Delta\boldsymbol{D}\varepsilon_2}{\lambda_1 - \lambda_2}\right)\varepsilon_2 + \left(\frac{\varepsilon_1^T\Delta\boldsymbol{D}\varepsilon_3}{\lambda_1 - \lambda_3}\right)\varepsilon_3. \quad [4]$$

The angle θ between the perturbed principal eigenvector of $\boldsymbol{D}$, $\boldsymbol{\epsilon}_1 + \Delta\boldsymbol{\epsilon}_1$, and the estimated eigenvector $\boldsymbol{\epsilon}_1$, can be approximated by $\theta = \tan^{-1}(\|\Delta\varepsilon_1\|)$. Using the small angle approximation (i.e., $\theta \approx \|\Delta\varepsilon_1\|$) and noting that the eigenvectors of $\boldsymbol{D}$ are mutually orthogonal, one can derive the root mean squared angular deviation from Eq. [4] (see Appendix B):

$$\theta_{RMS} = \sqrt{\langle\theta^2\rangle} \approx \sqrt{\langle\|\Delta\varepsilon_1\|^2\rangle} = \sqrt{\left(\frac{\varepsilon_1^T\Delta\boldsymbol{D}\varepsilon_2}{\lambda_1 - \lambda_2}\right)^2 + \left(\frac{\varepsilon_1^T\Delta\boldsymbol{D}\varepsilon_3}{\lambda_1 - \lambda_3}\right)^2}, \quad [5]$$

given $\lambda_1 > \lambda_2$ and $\lambda_1 > \lambda_3$.

One can compute the uncertainty of other tensor-derived quantities, such as the trace, FA, and RA, by apply-

ing error propagation theory (25). The variance of the Trace can be written as

$$\sigma^2_{Trace} \approx \sigma^2_{xxxx} + \sigma^2_{yyyy} + \sigma^2_{zzzz} + 2\sigma^2_{xxyy} + 2\sigma^2_{xxzz} + 2\sigma^2_{yyzz}$$

Exactly the same formula is obtained when it is assumed that the elements of the DT are distributed according to a multivariate Gaussian (14). Alternatively, we obtain:

$$\sigma^2_{Trace} \approx \sigma^2_{\lambda_1} + \sigma^2_{\lambda_2} + \sigma^2_{\lambda_3} + 2\sigma^2_{\lambda_{12}} + 2\sigma^2_{\lambda_{13}} + 2\sigma^2_{\lambda_{23}}. \quad [6]$$

The variance of each eigenvalues, $\sigma^2_{\lambda_1}$, $\sigma^2_{\lambda_2}$, *and* $\sigma^2_{\lambda_3}$, can be computed using Eq. [3] directly or obtained from the covariance matrix of eigenvalues, Σ_λ. However, the variance of covariance terms of eigenvalues, $\sigma^2_{\lambda_{12}}$, $\sigma^2_{\lambda_{13}}$, *and* $\sigma^2_{\lambda_{23}}$ must be obtained from Σ_λ which one can compute by applying the transformation matrix, $\boldsymbol{R}$, to the covariance matrix of tensors, i.,e., $\Sigma_\lambda = \boldsymbol{R}^T\Sigma_\alpha\boldsymbol{R}^T$ (17,23). To be more specific, we write $\sigma^2_{\lambda_1} = [\Sigma_\lambda]_{00}$, $\sigma^2_{\lambda_2} = [\Sigma_\lambda]_{11}$, $\sigma^2_{\lambda_3} = [\Sigma_\lambda]_{22}$, $\sigma^2_{\lambda_{12}} = [\Sigma_\lambda]_{01}$, $\sigma^2_{\lambda_{13}} = [\Sigma_\lambda]_{02}$, and $\sigma^2_{\lambda_{23}} = [\Sigma_\lambda]_{12}$. Note that we disagree with the covariance terms of eigenvalues derived in Ref. 17. Also, in contrast to the error propagation formulae presented in Ref. 18, the covariance terms that represent dependences between the difference eigenvalues appear in our formulae.

The variance of the FA can now be estimated by

$$\sigma^2_{FA} = \sigma^2_{\lambda_1}\left(\frac{\partial FA}{\partial\lambda_1}\right)^2 + \sigma^2_{\lambda_2}\left(\frac{\partial FA}{\partial\lambda_2}\right)^2 + \sigma^2_{\lambda_3}\left(\frac{\partial FA}{\partial\lambda_3}\right)^2 + 2\sigma^2_{\lambda_{12}}\frac{\partial FA}{\partial\lambda_1}\frac{\partial FA}{\partial\lambda_2} + 2\sigma^2_{\lambda_{13}}\frac{\partial FA}{\partial\lambda_1}\frac{\partial FA}{\partial\lambda_3} + 2\sigma^2_{\lambda_{23}}\frac{\partial FA}{\partial\lambda_2}\frac{\partial FA}{\partial\lambda_3} \quad [7]$$

where

$$FA = \frac{1}{\sqrt{2}}\sqrt{\frac{(\lambda_1-\lambda_2)^2 + (\lambda_1-\lambda_3)^2 + (\lambda_2-\lambda_3)^2}{\lambda_1^2+\lambda_2^2+\lambda_3^2}}.$$

And the uncertainty of the RA can be estimated by

$$\sigma^2_{RA} = \sigma^2_{\lambda_1}\left(\frac{\partial RA}{\partial\lambda_1}\right)^2 + \sigma^2_{\lambda_2}\left(\frac{\partial RA}{\partial\lambda_2}\right)^2 + \sigma^2_{\lambda_3}\left(\frac{\partial RA}{\partial\lambda_3}\right)^2 + 2\sigma^2_{\lambda_{12}}\frac{\partial RA}{\partial\lambda_1}\frac{\partial RA}{\partial\lambda_2} + 2\sigma^2_{\lambda_{13}}\frac{\partial RA}{\partial\lambda_1}\frac{\partial RA}{\partial\lambda_3} + 2\sigma^2_{\lambda_{23}}\frac{\partial RA}{\partial\lambda_2}\frac{\partial RA}{\partial\lambda_3} \quad [8]$$

where

$$RA = \frac{1}{\sqrt{2}}\frac{\sqrt{(\lambda_1-\lambda_2)^2 + (\lambda_1-\lambda_3)^2 + (\lambda_2-\lambda_3)^2}}{\lambda_1+\lambda_2+\lambda_3}.$$

Complete derivations of these expressions are provided in Appendix C.

MC Methods

Single Tensor Simulation

Simulations were performed following the approach previously described in Ref. 15 to obtain empirical estimates of the variance of various DT-derived quantities. The results were compared with the analytically derived values obtained with our method. Briefly, we simulated the effect of thermal noise in the DW signal intensities by generating complex random numbers whose real and imaginary parts were Gaussian-distributed with mean of 0 and standard deviation (SD) scaled to the desired SD of the signal. We then added the noise-free signal to the real part of the complex noise, and took the magnitude of this complex number to generate the noisy amplitude signal. DTs were computed from 16384 realizations of such noisy signals. We addressed several possible scenarios. We simulated cylindrically symmetric anisotropic DTs with diffusivity in the *x* direction set to two, three, five, and seven times the diffusivity in the *y* and *z* directions. The Trace of the DTs was representative of the Trace in brain parenchyma (2.1×10^{-3} mm^2/s). A study by Jones et al. (26) showed that the sampling scheme plays an important role in determining the uncertainty of the estimated tensors, and that at least 30 unique sampling orientations are required for rotationally invariant statistical properties of the estimated DT-derived quantities. Therefore, we tested the Jones 30 direction scheme with 35 *b*-values (five with $b = 0$, and 30 with $b = 1000$ s/mm^2) and different SNRs ranging from 5 to 100. The SNR is defined as the signal intensity in a $b = 0$ image divided by the signal SD. We also tested the same scheme with two, four, and eight replicates (70, 140, and 280 *b*-values). To validate the formulae using different gradient direction schemes, we tested six, 12, 20, 30, and 60 diffusion sampling directions with 65 *b*-values (five with $b = 0$, and 60 with $b = 1000$ s/mm^2). As indicated in Ref. 27, the tensor orientation affects the uncertainty measurement of tensor-derived quantities. Therefore, we tested three tensor orientations: the principal basis (i.e., three eigenvectors, one lying on each axis (*x*, *y*, *z*)), rotation around the *y*-axis at 45° from the principal basis, and rotation around the *x*-axis at 45° from the principal basis. The three eigenvalues in this simulation were set at 1500, 300, and 300 μm^2/s, with the SNR equal to 5, 10, and 20, respectively.

Brain Tissue Tensor Simulation

We also performed simulations to assess the validity of our analytic estimation of uncertainty in a situation representative of a clinical DTI scan of the brain. We collected a very high-quality DTI data set in the brain of a healthy male volunteer. Images were acquired with a DW-EPI sequence with $2 \times 2 \times 2$ mm^3 resolution and eight *b*-values ranging from 3 to 1200 s/mm^2. For each *b*-value, different directions were sampled following the "repulsion" scheme proposed by Jones et al. (26). The *b*-value (s/mm^2)/number of directions scheme was as follows: 3/3, 10/6, 65/10, 113/12, 350/16, 570/18, 850/20, and 1200/22. Each direction scheme was repeated seven times, and 749 DWI volumes per slice location were acquired (26,28). The total scan time was about 4 hr 40 min. All images were coregistered (29) and the RESTORE tensor fitting approach (30) was used to obtain a robust estimation of all tensor elements. We considered the DT computed at each voxel location in the brain from this high-quality data set to be an error-free measurement of water diffusivity. From this DT and a given experimental design (an assumed set of

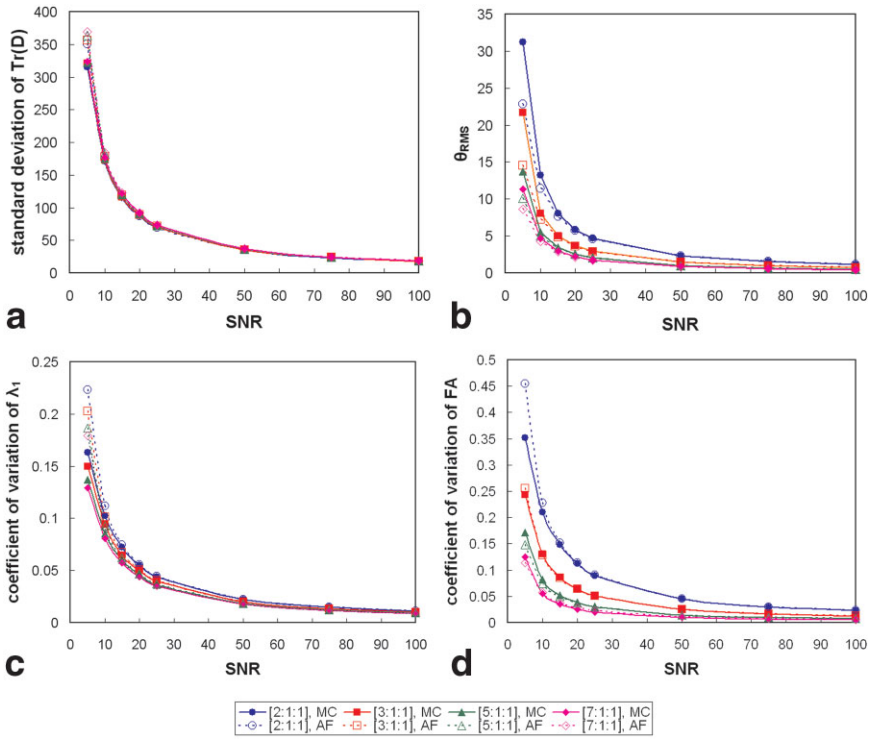

FIG. 1. (**a**) The SD of trace; (**b**) the RMS of the perturbed first eigenvector, θ_{RMS}; (**c**) the COV of the first eigenvalue, λ_1; and (**d**) the COV of FA, computed using MC methods and AF for different SNRs with various predefined anisotropic DTs (λ_1:λ_2:λ_3 with trace = 2100 μm^2/s) and 35 *b*-values (5 with $b = 0$ and 30 with $b = 1000$ s/mm^2).

b-matrices), we then produced noise-free synthetic DW images and computed the signal intensity in each voxel using the formula (21): $S_{(\boldsymbol{b})} = S_{(0)} * \exp(-\boldsymbol{b} : \boldsymbol{D})$, where $\boldsymbol{D}$ is the DT, $\boldsymbol{b}$ is the desired b matrix, and S_0 is the amplitude image intensity.

For this simulation using human brain data we tested only Jones 30 gradient direction scheme: with $b = 1000$ plus five non-DW images. We also added Gaussian-distributed noise in quadrature to simulate images with an SNR of 20 measured in the thalamus of the $b = 0$ image. We then computed the DT using the synthetic human brain data created by nonlinear regression. We repeated this procedure 500 times and used the results to estimate the uncertainty of the DT and its derived quantities in each voxel. We also created 20 replicates of such data set to be used for bootstrapping for cross-validation. We computed the DT 1000 times to obtain the SD for the DT-derived quantities.

RESULTS

Figure 1 shows the SDs of Trace (σ_{Trace}), the root mean square (RMS) angular deviation (θ_{RMS}), the coefficient of variation (COV) of the largest eigenvalue ($\sigma_{\lambda_1}/\langle\lambda_1\rangle$), and the COV of the FA ($\sigma_{FA}/\langle FA\rangle$), computed using MC methods and the analytic formulae (AF) given in Eqs. [3] and [5]–[7], for different SNRs (ranging from 5 to 100) and with different anisotropic DTs (the ratio of λ_1:λ_2:λ_3 = 2:1:1, 3:1:1, 5:1:1, and 7:1:1, which has FA = 0.41, 0.60, 0.77, and 0.84, respectively). The Trace in the simulation was set to 2.1×10^{-3} mm^2/s, which is representative of the trace of brain parenchyma. The 30-gradient scheme with $b = 1000$ s/mm^2 and five non-DW images was used. The trends of SD in the MC and AF are consistent for all estimated parameters. The difference in σ_{Trace} between the MC and AF is negligible, with an error of <5% in all of the anisotropic cases we tested when the SNR is greater than 10. The difference of θ_{RMS} is negligible, with an error of <5% when the SNR is greater than 20. The differences of the COV of FA and the largest eigenvalue are negligible with error less than 3% and 5%, respectively, when the SNR is greater than 15. For SNR = 5, the error will be larger and sensitive to the degree of anisotropy. Both empirical and analytical methods predict a power law scaling relationship: $\sigma_{Trace} \propto \text{SNR}^{-1}$, $\sigma_{\lambda_1} \propto \text{SNR}^{-1}$, $\sigma_{FA} \propto \text{SNR}^{-1}$, and $\theta_{\text{RMS}} \propto \text{SNR}^{-1}$. These scaling results are generated using the MC method, but are analytically derivable from the formulae given in the previous section.

Figure 2 shows that the estimated θ_{RMS} decreases as more DW images are used, and again the trends for the MC and AF are consistent. The results shown here are for an anisotropic tensor with λ_1:λ_2:λ_3 = 1500:300:300 μm^2/s. Both approaches also predict a power law scaling relationship, $\theta_{\text{RMS}} \propto N^{-1}$, where N is the number of DW replicates. Other tensor-derived parameters, such as the Trace, principal eigenvalue, and FA, also exhibit the same trend (data not shown here).

Figure 3 shows the estimated SD of the FA for selected slices in human brain using MC (upper panel) and AF (middle panel). The lower panel is the absolute difference map between the MC and AF estimates. The AF provides a precise uncertainty estimation of FA in most brain areas, especially in high anisotropic areas. The difference between AF and MC is higher in isotropic areas, such as the CSF-filled ventricles. Given the SNR = 20 in this example, the estimate of σ_{FA} from the AF is 23.5% on average, which is lower than the estimate of σ_{FA} from MC in the selected CSF region shown in Fig. 3. The SD maps of the trace using MC and AF are very similar,

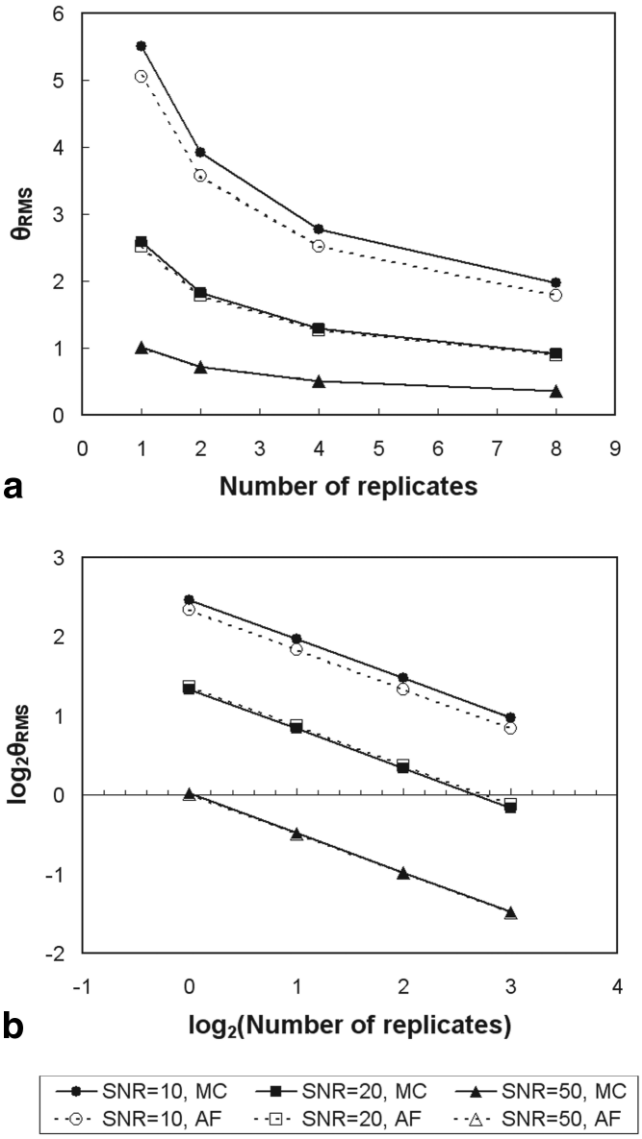

FIG. 2. (**a**) The RMS of the perturbed angle, θ_{RMS}, and (**b**) the logarithmic transform of θ_{RMS}, $\log_2(\theta_{RMS})$, using MC methods and AF for different SNRs with predefined anisotropic DTs (λ_1:λ_2:λ_3 = 1500:300:300 $\mu m^2/s$) and different numbers of replicates (one replicate consists of five $b = 0$ and 30 $b = 1000$ s/mm^2).

with a maximum error of <5% (data not shown here). The results of bootstrapping are consistent with the results of the MC simulation.

Figure 4 shows the estimated SD of the FA and RA, the ratio σ_{FA}/σ_{RA}, and the ratio SNR(FA)/SNR(RA) = $(FA/\sigma_{FA})/(RA/\sigma_{RA})$ using the AF for different SNRs with different degrees of anisotropy ranging from 0 to 1. The measure used to quantify diffusion anisotropy is C_{linear}, proposed by Westin et al. (31), which is defined as $C_{linear} = \frac{\lambda_1 - \lambda_3}{\lambda_1 + \lambda_2 + \lambda_3}$, where λ_1, λ_2, and λ_3 are the rank-sorted eigenvalues of the DT. The estimated σ_{FA} and σ_{RA} both decrease as the SNR is increased. The estimated σ_{FA} decreases as C_{linear} increases, while the estimated σ_{RA} increases as C_{linear} increases. However, consistent with the result reported in Ref. 32, the ratio σ_{FA}/σ_{RA} and SNR(FA)/SNR(RA) are both independent of SNR. Figure 4 also demonstrates that the FA has superior noise immunity relative to the RA. Note that the predictions of our AF agree exactly with the formula given by Hasan et al. (32), who derived the relationship between the ratio of FA and RA, and the ratio of σ_{FA} and σ_{RA}. However, Hasan et al. (32) did not provide individual expressions for σ_{FA} or σ_{RA}. We show in Fig. 4a and b that our AF yield σ_{FA} and σ_{RA} directly. In Fig. 4c and d, the ratio σ_{FA}/σ_{RA} and SNR(FA)/SNR(RA), computed exactly from the data provided in Fig. 4a and b, are identical to Hasan et al.'s (32) formulae: $\sigma_{FA}/\sigma_{RA} = (1/3)(FA/RA)^3$ and $SNR(FA)/SNR(RA) = 1 + RA^2$ (32).

Figure 5 shows the estimate of σ_{FA} for various numbers of gradient directions. Given the same tensor orientation (the diagonal tensor in this example), the same number of images for each scheme (60 DW images and five $b = 0$ images in this example), and the same SNR, the gradient direction scheme has very little effect on the uncertainty measurement of FA. Other diffusion-derived quantities, such as the trace and RA, behave similarly (data not shown here).

DISCUSSION

The results show the proposed AF accurately estimate the uncertainty of the tensor and its derived quantities over a useful range of SNRs and experimental designs. However, for extremely low SNRs (<5), reliable results are not expected because at low SNR, several of the simplifying assumptions may not hold. For example, when the SNR is low, the angular excursion about the mean eigenvector is large, so the small angle approximation will no longer be satisfied. The assumptions of the first-order perturbation theory (e.g., that the SD is small compared to the mean tensor) may also not be satisfied. As indicated by Jones (33), when the diffusion attenuation is high ($b > 3000$ s/mm^2) and/or the SNR is low (<5), the noise floor is sampled, which creates artifacts in the DW image. These AF are therefore not recommended when the DWI experiments are potentially prone to this artifact. As shown in Figs. 1–3 and 5, the AF and simulations give similar results in estimating the uncertainty in tensor-derived indices with SNR > 10 and a clinical b-value ($b = 1000$ s/mm^2) regardless of the gradient sampling scheme used and the number of replicates acquired.

The AF are useful for designing DTI experiments for certain applications and for analyzing the DTI data. Although the MC simulation has similar applications, it is time-consuming and may not be practical for clinicians. For example, to obtain a reliable estimate of Trace with a 95% confidence interval (CI) from a stroke patient, would a six-gradient direction scheme with $b = 1000$ s/mm^2 and one $b = 0$ image be sufficient? Assuming that the measured SNR in the thalamus of the $b = 0$ image is about 20, the answer is no, since only a 90% CI on the Trace is achieved. Then the question would be, how many replicates should be acquired or how should a scheme with more gradient directions be used instead? The answer using the AF is straightforward: either four replicates should be acquired if the six-gradient-directions scheme with one $b = 0$ is used, or the 30-gradient-directions scheme with three $b =$

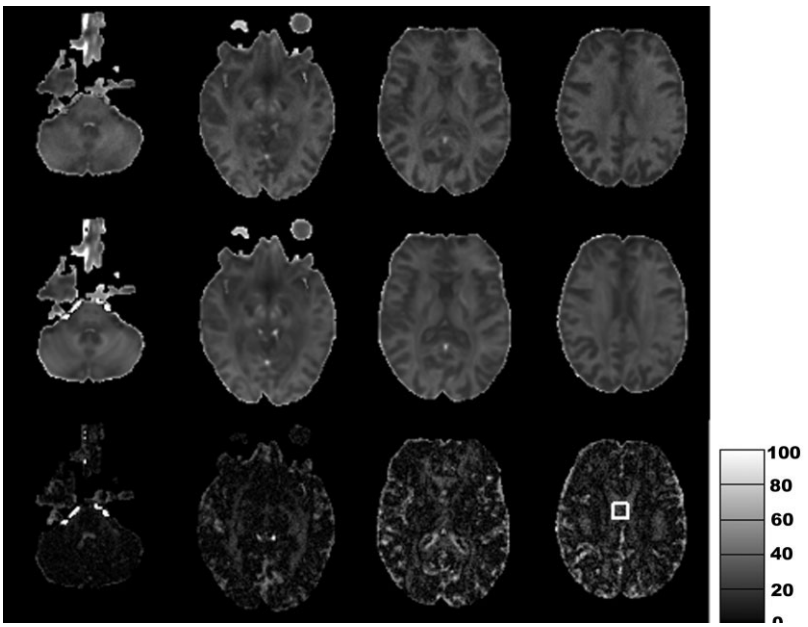

FIG. 3. The estimated SD of FA of selected slices of human brain using MC (Row 1) and AF (Row 2). The lower panel is the absolute difference map between MC and AF. A square region marked in the last image of the lower panel indicates that a larger error (23.5%) occurred in the CSF-filled area (the color bar applies only to the Row 3).

0 images should be used. Another example is to quantify the reliability of tractography findings. It is known that the computed trajectory always deviates from the true trajectory due to noise. This has been demonstrated with the use of simulation (34,35) and bootstrapping (27,36). Although the cone of uncertainty map (36) and the confidence map (27) constructed using bootstrapping can quantify the uncertainty of an eigenvector in each voxel and assign confidence to the tracking result, they may not be practical for clinical studies. It is also difficult to determine how large the superset should be and how small the subset should be to reach a reliable assessment. The AF provide a novel way to construct such maps explicitly and obtain an overall notion of the reliability of estimated parameters. However, it should be noted that these formulae were derived from the linear least-squares model, and only the Gaussian RF noise was taken into account. In reality, physiological artifacts, such as subject motion or cardiac pulsation, eddy-current distortion, and phase error, could affect the uncertainty measurement and cause higher uncertainty in measured quantities in general. Empirical methods, such as the bootstrap, would be more suitable and valuable for dealing with uncertainty when such artifacts are present in data.

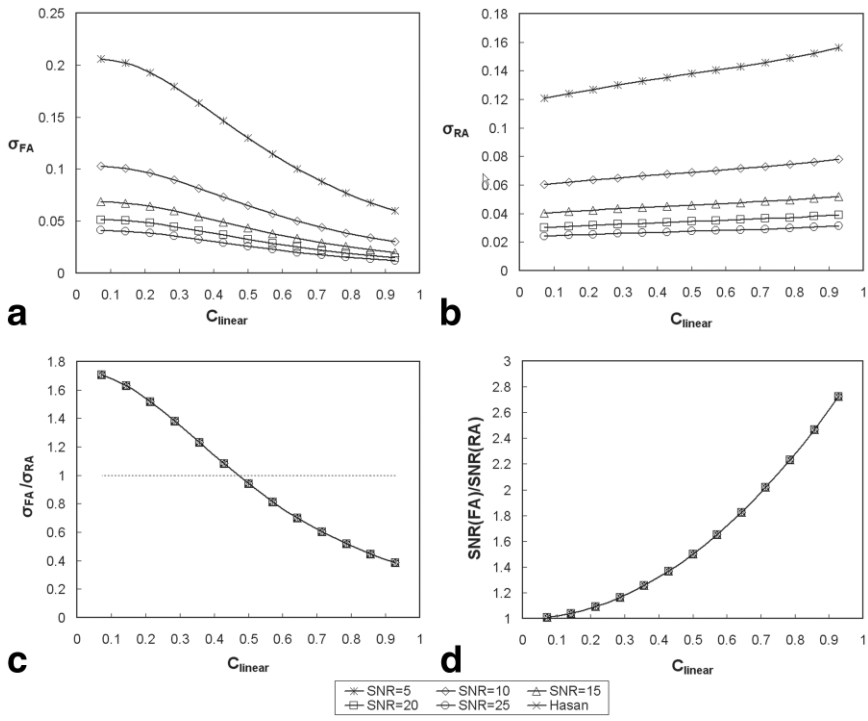

FIG. 4. The estimated SD of (**a**) FA and (**b**) RA using the proposed AF, (**c**) the ratio of σ_{FA}/σ_{RA} using the AF and Hasan et al.'s (32) formula $\sigma_{FA}/\sigma_{RA} = (1/3)(FA/RA)^3$, and (**d**) the ratio of SNR(FA)/SNR(RA) using AF and Hasan et al.'s (32) formula $SNR(FA)/SNR(RA) = 1 + RA^2$ (32) for different SNRs with various anisotropic DTs ($C_{linear} = 0$–1).

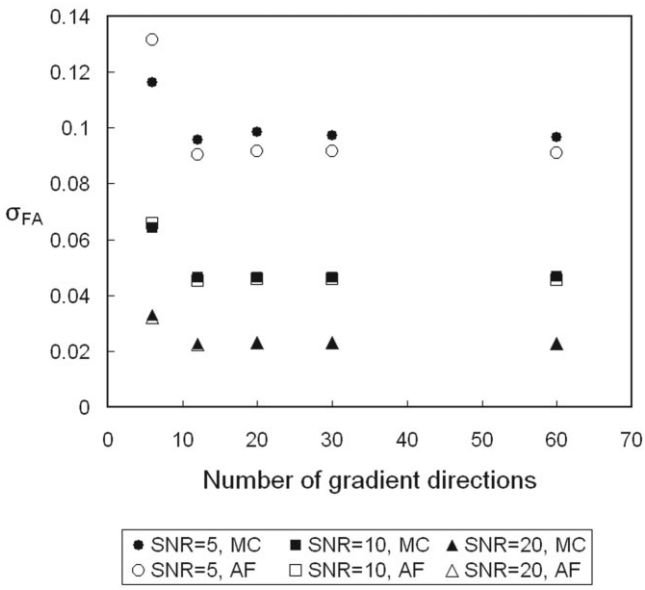

FIG. 5. The estimated SD of FA, σ_{FA}, using MC and AF for various gradient direction schemes with SNR = 5, 10, and 20.

As indicated in Fig. 3, the AF for the uncertainty of FA are more susceptible to error in isotropic regions (e.g., CSF-filled ventricles) because eigenvalues and eigenvectors become singular as the condition for isotropy is approached. However, since these quantities are typically important primarily where the degree of diffusion anisotropy or FA is high, such as in WM pathways, in practice this inaccuracy may not matter.

It should be noted that covariance terms arising in the error propagation formula should not be ignored. In general, the first two terms (see Eq. [C1]) dominate the uncertainties; however, in previous studies the covariance terms were neglected (18,37). When fluctuations in the measured quantities are uncorrelated, the covariance terms are expected to vanish. However, if the fluctuations in the measured quantities are correlated, it is unclear what bias will arise from neglecting those covariance terms. In fact, the covariance terms often make significant contributions to the uncertainties in parameters determined by fitting curves to data by the least-squares method (25). The tensor-fitting procedure uses the least-squares approach, and the derived eigenvalues are not independent. The error propagation approach used here to derive the uncertainty of other tensor indices, such as the trace and FA, takes the covariance terms into account but neglects higher-order terms in the Taylor expansion, as shown in Appendix C. When the errors are large, at least the second partial derivatives and partial cross derivative must be included. This may partly explain why the current results are so robust. We observed from the simulations that the uncertainty measurements on the FA and RA were about 7–10% lower when the covariance terms were ignored.

The results presented in the previous section were obtained with a diagonal tensor in both the simulation and formulae. As indicated in Ref. 27, the tensor orientation can affect the uncertainty measurement of tensor-derived quantities to different degrees when different gradient schemes are used. Previous studies (12,37,38) compared the gradient sampling schemes for measuring DTI-derived quantities with the use of simulations. In this work we tested only a few tensor orientations and five different gradient sampling schemes to demonstrate that the proposed formulae take into consideration tensor orientation or imaging gradient cross-terms, and are valid for different gradient sampling schemes.

CONCLUSIONS

For any imaginable application of DTI, it is necessary to assess the variance of the DT and tensor-derived quantities. The perturbation approach for estimating the uncertainty in the DT and its derived quantities is a powerful tool for DTI data analysis and experimental design. In this study we validated the AF using MC methods, and compared the results with previous findings.

Although the parametric statistical analysis described by Pajevic and Basser (13) does provide a robust estimate for the distribution of Trace, it only provides estimates of the distribution of other tensor-derived quantities under very restrictive assumptions, i.e., that the tensor is estimated using an unweighted linear least-squares model (which is not the case), and that an isotropic gradient scheme is used to acquire the DWI data. Empirical methods, such as the bootstrap, can provide the distribution of any tensor-derived variable or parameter of interest; however, such methods require additional DWI data and thus can be prohibitively expensive or even unethical for treating certain patients.

We believe that analytical estimation of the uncertainty of DTI-derived parameters is easy to implement and provides acceptable accuracy for many clinical DTI applications.

ACKNOWLEDGMENTS

The authors thank Dr. Sinisa Pajevic for helpful discussion, Dr. Stefano Marenco for acquiring the human brain data set, and Ms. Liz Salak for editing the manuscript. This research was supported by the Intramural Research Program of the National Institute of Child Health and Human Development.

APPENDIX A

Let $\boldsymbol{D_0}$ be a real, symmetric 3×3 matrix and let $\boldsymbol{\Delta D}$ be a real, symmetric perturbation matrix. Let $\boldsymbol{\epsilon}_i$ and λ_i, $\{i = 1, 2, 3\}$ be the eigenvectors and eigenvalues, respectively, of $\boldsymbol{D_0}$. Assume that the λ_i are distinct. We wish to obtain a first-order approximation of the eigenvectors and eigenvalues of $\boldsymbol{D}$ in terms of the $\boldsymbol{\epsilon}_i$ and λ_i, where $\boldsymbol{D} = \boldsymbol{D_0} + \boldsymbol{\Delta D}$, and $\boldsymbol{D\epsilon} = \boldsymbol{\lambda D}$. These may be obtained by retaining the terms of first order or lower of the equation $(\boldsymbol{D_0} + \boldsymbol{\Delta D})(\boldsymbol{\epsilon_i} + \boldsymbol{\Delta\epsilon_i}) = (\lambda_i + \Delta\lambda_i)(\boldsymbol{\epsilon_i} + \boldsymbol{\Delta\epsilon_i})$, where $\boldsymbol{D_0}\,\boldsymbol{\epsilon_i} = \lambda_i\,\boldsymbol{\epsilon_i}$. The resulting equation is

$$\boldsymbol{D_0}\Delta\varepsilon_i + \Delta\boldsymbol{D}\varepsilon_i \approx \lambda_i\Delta\varepsilon_i + \Delta\lambda_i\varepsilon_i. \qquad [A1]$$

To calculate $\Delta\lambda_i$, we can premultiply Eq. [A1] by $\boldsymbol{\epsilon_i^T}$.

$$\varepsilon_i^T\boldsymbol{D_0}\Delta\varepsilon_i + \varepsilon_i^T\Delta\boldsymbol{D}\varepsilon_i \approx \varepsilon_i^T\lambda_i\Delta\varepsilon_i + \varepsilon_i^T\Delta\lambda_i\varepsilon_i.$$

Since $\varepsilon_i^T \mathbf{D_0} = \lambda_i \varepsilon_i^T$, $\mathbf{D_0}\varepsilon_i = \lambda_i \varepsilon_i$, and $\varepsilon_i^T \varepsilon_j = 0$, we have

$$\Delta\lambda_i \approx \varepsilon_i^T \Delta \mathbf{D} \varepsilon_i. \quad [A2]$$

Since ϵ_1, ϵ_2, and ϵ_3 form a complete set of basis vectors, we can write $\Delta\epsilon_i$ as a linear combination of the ϵ_j as follows:

$$\Delta\varepsilon_i = \sum_{j=1}^{3} \beta_{ij}\varepsilon_j, \text{ where } \beta_{ij} = \varepsilon_j^T \Delta\varepsilon_i. \quad [A3]$$

If we premultiply Eq. [A1] by ϵ_j^T and rearrange terms, we obtain

$$\beta_{ij} = \begin{cases} \dfrac{\varepsilon_j^T \Delta D \varepsilon_i}{\lambda_i - \lambda_j} & \text{for } i \neq j \\ 0 & \text{for } i = j \end{cases} \quad [A4]$$

A similar derivation can be also found in Ref. 24.

APPENDIX B

From Eqs. [A3] and [A4], we have

$$\Delta\varepsilon_1 = \left(\frac{\varepsilon_1^T \Delta D \varepsilon_2}{\lambda_1 - \lambda_2}\right)\varepsilon_2 + \left(\frac{\varepsilon_1^T \Delta D \varepsilon_3}{\lambda_1 - \lambda_3}\right)\varepsilon_3, \quad [B1]$$

where $\lambda_1 > \lambda_2$ and $\lambda_1 > \lambda_3$. The angle θ between $\epsilon_1 + \Delta\epsilon_1$ and ϵ_1, can be computed by $\theta = \tan^{-1}(\|\Delta\varepsilon_1\|)$. Using the small angle approximation, one can rewrite the formula $\theta \approx \|\Delta\varepsilon_1\|$. The root mean squared angular deviation from the mean principal direction, Θ_{RMS}, can be estimated by

$$\begin{aligned} \theta_{RMS} &= \sqrt{\langle\theta^2\rangle} \approx \sqrt{\langle\|\Delta\varepsilon_1\|^2\rangle} \\ &= \sqrt{\left\langle \left(\left(\frac{\varepsilon_1^T \Delta D \varepsilon_2}{\lambda_1 - \lambda_2}\right)\varepsilon_2 + \left(\frac{\varepsilon_1^T \Delta D \varepsilon_3}{\lambda_1 - \lambda_3}\right)\varepsilon_3 \right)^2 \right\rangle}. \\ &= \sqrt{\left(\frac{\varepsilon_1^T \Delta D \varepsilon_2}{\lambda_1 - \lambda_2}\right)^2 + \left(\frac{\varepsilon_1^T \Delta D \varepsilon_3}{\lambda_1 - \lambda_3}\right)^2} \end{aligned} \quad [B2]$$

The eigenvalues and eigenvectors can be computed from the data, and the perturbation matrix of tensors can be estimated from the data as well. The approximation of $\Delta\mathbf{D}$ is described in Materials and Methods, and can also be found in Ref. 17.

APPENDIX C

Suppose we want to determine a quantity x that is a function of at least two measured variables, u and v:

$$x = f(u, v, \ldots).$$

.

The general form for the propagation of errors is

$$(\sigma_x)^2 \approx \sigma_u^2\left(\frac{\partial x}{\partial u}\right)^2 + \sigma_v^2\left(\frac{\partial x}{\partial v}\right)^2 + \ldots + 2\sigma_{uv}^2\left(\frac{\partial x}{\partial u}\right)\left(\frac{\partial x}{\partial v}\right) + \ldots. \quad [C1]$$

The definition of the scalar invariant indices can be written as:

$$I_1 = \lambda_1 + \lambda_2 + \lambda_3 = Trace(\mathbf{D})$$

$$I_2 = \lambda_1\lambda_2 + \lambda_1\lambda_3 + \lambda_2\lambda_3$$

$$I_3 = \lambda_1\lambda_2\lambda_3$$

$$I_4 = \lambda_1^2 + \lambda_2^2 + \lambda_3^2.$$

By applying the error propagation formula (Eq. [C1]), one can obtain the variance of trace:

$$\begin{aligned} \sigma_{Trace}^2 \approx{}& \sigma_{\lambda_1}^2\left(\frac{\partial I_1}{\partial\lambda_1}\right)^2 + \sigma_{\lambda_2}^2\left(\frac{\partial I_1}{\partial\lambda_2}\right)^2 + \sigma_{\lambda_3}^2\left(\frac{\partial I_1}{\partial\lambda_3}\right)^2 + 2\sigma_{\lambda_1\lambda_2}^2\left(\frac{\partial I_1}{\partial\lambda_1}\right) \\ &\times\left(\frac{\partial I_1}{\partial\lambda_2}\right) + 2\sigma_{\lambda_1\lambda_3}^2\left(\frac{\partial I_1}{\partial\lambda_1}\right)\left(\frac{\partial I_1}{\partial\lambda_3}\right) + 2\sigma_{\lambda_2\lambda_3}^2\left(\frac{\partial I_1}{\partial\lambda_2}\right)\left(\frac{\partial I_1}{\partial\lambda_3}\right) \end{aligned} \quad [c2]$$

$$\sigma_{Trace}^2 \approx \sigma_{\lambda_1}^2 + \sigma_{\lambda_2}^2 + \sigma_{\lambda_3}^2 + 2\sigma_{\lambda_{12}}^2 + 2\sigma_{\lambda_{13}}^2 + 2\sigma_{\lambda_{23}}^2. \quad [C3]$$

For FA and RA, a similar approach can be used. The FA can be rewritten as

$$FA = \frac{1}{\sqrt{2}}\sqrt{\frac{(\lambda_1 - \lambda_2)^2 + (\lambda_1 - \lambda_3)^2 + (\lambda_2 - \lambda_3)^2}{\lambda_1^2 + \lambda_2^2 + \lambda_3^2}} = \sqrt{\frac{I_4 - I_2}{I_4}}.$$

The estimated variance of FA is

$$\begin{aligned} \sigma_{FA}^2 = {}& \sigma_{\lambda_1}^2\left(\frac{\partial FA}{\partial\lambda_1}\right)^2 + \sigma_{\lambda_2}^2\left(\frac{\partial FA}{\partial\lambda_2}\right)^2 + \sigma_{\lambda_3}^2\left(\frac{\partial FA}{\partial\lambda_3}\right)^2 \\ &+ 2\sigma_{\lambda_{12}}^2\frac{\partial FA}{\partial\lambda_1}\frac{\partial FA}{\partial\lambda_2} + 2\sigma_{\lambda_{13}}^2\frac{\partial FA}{\partial\lambda_1}\frac{\partial FA}{\partial\lambda_3} + 2\sigma_{\lambda_{23}}^2\frac{\partial FA}{\partial\lambda_2}\frac{\partial FA}{\partial\lambda_3} \end{aligned} \quad [C4]$$

where

$$\begin{aligned} \frac{\partial FA}{\partial\lambda_1} &= \left(\lambda_1 - \frac{\lambda_2 + \lambda_3}{2}\right)\frac{1}{\sqrt{I_4(I_4 - I_2)}} - \lambda_1\frac{\sqrt{I_4 - I_2}}{\sqrt{I_4^3}} \\ &= \left(\frac{3\lambda_1 - I_1}{2}\right)\frac{1}{\sqrt{I_4(I_4 - I_2)}} - \lambda_1\frac{\sqrt{I_4 - I_2}}{\sqrt{I_4^3}} \end{aligned}$$

$$\begin{aligned} \frac{\partial FA}{\partial\lambda_2} &= \left(\lambda_2 - \frac{\lambda_1 + \lambda_3}{2}\right)\frac{1}{\sqrt{I_4(I_4 - I_2)}} - \lambda_2\frac{\sqrt{I_4 - I_2}}{\sqrt{I_4^3}} \\ &= \left(\frac{3\lambda_2 - I_1}{2}\right)\frac{1}{\sqrt{I_4(I_4 - I_2)}} - \lambda_2\frac{\sqrt{I_4 - I_2}}{\sqrt{I_4^3}} \end{aligned}$$

$$\begin{aligned} \frac{\partial FA}{\partial\lambda_3} &= \left(\lambda_3 - \frac{\lambda_1 + \lambda_2}{2}\right)\frac{1}{\sqrt{I_4(I_4 - I_2)}} - \lambda_3\frac{\sqrt{I_4 - I_2}}{\sqrt{I_4^3}} \\ &= \left(\frac{3\lambda_3 - I_1}{2}\right)\frac{1}{\sqrt{I_4(I_4 - I_2)}} - \lambda_3\frac{\sqrt{I_4 - I_2}}{\sqrt{I_4^3}}. \end{aligned}$$

The RA can be rewritten as

$$RA = \frac{1}{\sqrt{2}} \frac{\sqrt{(\lambda_1 - \lambda_2)^2 + (\lambda_1 - \lambda_3)^2 + (\lambda_2 - \lambda_3)^2}}{\lambda_1 + \lambda_2 + \lambda_3} = \frac{\sqrt{I_4 - I_2}}{I_1}.$$

The estimated variance of RA is

$$\sigma_{RA}^2 = \sigma_{\lambda_1}^2 \left(\frac{\partial RA}{\partial \lambda_1} \right)^2 + \sigma_{\lambda_2}^2 \left(\frac{\partial RA}{\partial \lambda_2} \right)^2 + \sigma_{\lambda_3}^2 \left(\frac{\partial RA}{\partial \lambda_3} \right)^2 + 2\sigma_{\lambda_{12}}^2 \frac{\partial RA}{\partial \lambda_1} \frac{\partial RA}{\partial \lambda_2} + 2\sigma_{\lambda_{13}}^2 \frac{\partial RA}{\partial \lambda_1} \frac{\partial RA}{\partial \lambda_3} + 2\sigma_{\lambda_{23}}^2 \frac{\partial RA}{\partial \lambda_2} \frac{\partial RA}{\partial \lambda_3} \quad [C5]$$

where

$$\frac{\partial RA}{\partial \lambda_1} = \left(\left(\lambda_1 - \frac{\lambda_2 + \lambda_3}{2} \right) \frac{1}{I_1 \sqrt{I_4 - I_2}} - \frac{\sqrt{I_4 - I_2}}{I_1^2} \right) = \left(\left(\frac{3\lambda_1 - I_1}{2} \right) \frac{1}{I_1 \sqrt{I_4 - I_2}} - \frac{\sqrt{I_4 - I_2}}{I_1^2} \right)$$

$$\frac{\partial RA}{\partial \lambda_2} = \left(\left(\lambda_2 - \frac{\lambda_1 + \lambda_3}{2} \right) \frac{1}{I_1 \sqrt{I_4 - I_2}} - \frac{\sqrt{I_4 - I_2}}{I_1^2} \right) = \left(\left(\frac{3\lambda_2 - I_1}{2} \right) \frac{1}{I_1 \sqrt{I_4 - I_2}} - \frac{\sqrt{I_4 - I_2}}{I_1^2} \right)$$

$$\frac{\partial RA}{\partial \lambda_3} = \left(\left(\lambda_3 - \frac{\lambda_1 + \lambda_2}{2} \right) \frac{1}{I_1 \sqrt{I_4 - I_2}} - \frac{\sqrt{I_4 - I_2}}{I_1^2} \right) = \left(\left(\frac{3\lambda_3 - I_1}{2} \right) \frac{1}{I_1 \sqrt{I_4 - I_2}} - \frac{\sqrt{I_4 - I_2}}{I_1^2} \right)$$

REFERENCES

1. Moseley ME, Butts K, Yenari MA, Marks M, de Crespigny A. Clinical aspects of DWI. NMR Biomed 1995;8:387–396.
2. Pierpaoli C, Barnett A, Pajevic S, Chen R, Penix LR, Virta A, Basser P. Water diffusion changes in Wallerian degeneration and their dependence on white matter architecture. Neuroimage 2001;13(6 Pt 1):1174–1185.
3. Horsfield MA, Larsson HB, Jones DK, Gass A. Diffusion magnetic resonance imaging in multiple sclerosis. J Neurol Neurosurg Psychiatry 1998;64(Suppl 1):S80–84.
4. Goldberg-Zimring D, Mewes AU, Maddah M, Warfield SK. Diffusion tensor magnetic resonance imaging in multiple sclerosis. J Neuroimaging 2005;15(Suppl):68S–81S.
5. Moseley M. Diffusion tensor imaging and aging—a review. NMR Biomed 2002;15:553–560.
6. Pajevic S, Pierpaoli C. Color schemes to represent the orientation of anisotropic tissues from diffusion tensor data: application to white matter fiber tract mapping in the human brain. Magn Reson Med 1999; 42:526–540.
7. Mori S, van Zijl PC. Fiber tracking: principles and strategies—a technical review. NMR Biomed 2002;15:468–480.
8. Yu CS, Li KC, Xuan Y, Ji XM, Qin W. Diffusion tensor tractography in patients with cerebral tumors: a helpful technique for neurosurgical planning and postoperative assessment. Eur J Radiol 2005;56:197–204.
9. Lori NF, Akbudak E, Shimony JS, Cull TS, Snyder AZ, Guillory RK, Conturo TE. Diffusion tensor fiber tracking of human brain connectivity: acquisition methods, reliability analysis and biological results. NMR Biomed 2002;15:494–515.
10. Evans AC. The NIH MRI study of normal brain development. Neuroimage 2006;30:184–202.
11. Mukherjee P, Bahn MM, McKinstry RC, Shimony JS, Cull TS, Akbudak E, Snyder AZ, Conturo TE. Differences between gray matter and white matter water diffusion in stroke: diffusion-tensor MR imaging in 12 patients. Radiology 2000;215:211–220.
12. Jones DK. The effect of gradient sampling schemes on measures derived from diffusion tensor MRI: a Monte Carlo study. Magn Reson Med 2004;51:807–815.
13. Pajevic S, Basser PJ. Parametric and non-parametric statistical analysis of DT-MRI data. J Magn Reson 2003;161:1–14.
14. Basser PJ, Pajevic S. Dealing with uncertainty in diffusion tensor MR data. Israel J Chem 2003;43:129–144.
15. Pierpaoli C, Basser PJ. Toward a quantitative assessment of diffusion anisotropy. Magn Reson Med 1996;36:893–906.
16. Basser PJ. Quantifying errors in fiber direction and diffusion tensor field maps resulting from MR noise. In: Proceedings of the 5th Annual Meeting of ISMRM, Vancouver, Canada, 1997 (Abstract 1740).
17. Anderson AW. Theoretical analysis of the effects of noise on diffusion tensor imaging. Magn Reson Med 2001;46:1174–1188.
18. Poonawalla AH, Zhou XJ. Analytical error propagation in diffusion anisotropy calculations. J Magn Reson Imaging 2004;19:489–498.
19. Skare S, Hedehus M, Moseley ME, Li TQ. Condition number as a measure of noise performance of diffusion tensor data acquisition schemes with MRI. J Magn Reson 2000;147:340–352.
20. Skare S, Li T, Nordell B, Ingvar M. Noise considerations in the determination of diffusion tensor anisotropy. Magn Reson Imaging 2000;18: 659–669.
21. Basser PJ, Mattiello J, LeBihan D. Estimation of the effective self-diffusion tensor from the NMR spin echo. J Magn Reson B 1994;103: 247–254.
22. Mattiello J, Basser PJ, Le Bihan D. The b matrix in diffusion tensor echo-planar imaging. Magn Reson Med 1997;37:292–300.
23. Hext GR. The estimation of second-order tensors, with related test and design. Biometrika 1963;50:353–373.
24. Fukunaga K. Introduction to statistical pattern recognition. New York: Academic Press Inc.; 1972.
25. Bevington P. Data reduction and error analysis for the physical sciences. New York: McGraw-Hill Book Company; 1969.
26. Jones DK, Horsfield MA, Simmons A. Optimal strategies for measuring diffusion in anisotropic systems by magnetic resonance imaging. Magn Reson Med 1999;42:515–525.
27. Jones DK, Pierpaoli C. Confidence mapping in diffusion tensor magnetic resonance imaging tractography using a bootstrap approach. Magn Reson Med 2005;53:1143–1149.
28. Pierpaoli C, Jones DK. Removing CSF contamination in brain DT-MRIs by using a two-compartment tensor model. In: Proceedings of the 12th Annual Meeting of ISMRM, Kyoto, Japan, 2004. (Abstract 1215)
29. Rohde GK, Barnett AS, Basser PJ, Marenco S, Pierpaoli C. Comprehensive approach for correction of motion and distortion in diffusion-weighted MRI. Magn Reson Med 2004;51:103–114.
30. Chang LC, Jones DK, Pierpaoli C. RESTORE: robust estimation of tensors by outlier rejection. Magn Reson Med 2005;53:1088–1095.
31. Westin CF, Maier SE, Mamata H, Nabavi A, Jolesz FA, Kikinis R. Processing and visualization for diffusion tensor MRI. Med Image Anal 2002;6:93–108.
32. Hasan KM, Alexander AL, Narayana PA. Does fractional anisotropy have better noise immunity characteristics than relative anisotropy in diffusion tensor MRI? An analytical approach. Magn Reson Med 2004; 51:413–417.
33. Jones DK, Basser PJ. "Squashing peanuts and smashing pumpkins": how noise distorts diffusion-weighted MR data. Magn Reson Med 2004; 52:979–993.
34. Basser PJ, Pajevic S, Pierpaoli C, Duda J, Aldroubi A. In vivo fiber tractography using DT-MRI data. Magn Reson Med 2000;44:625–632.
35. Lazar M, Alexander AL. An error analysis of white matter tractography methods: synthetic diffusion tensor field simulations. Neuroimage 2003;20:1140–1153.
36. Jones DK. Determining and visualizing uncertainty in estimates of fiber orientation from diffusion tensor MRI. Magn Reson Med 2003;49:7–12.
37. Papadakis NG, Xing D, Houston GC, Smith JM, Smith MI, James MF, Parsons AA, Huang CL, Hall LD, Carpenter TA. A study of rotationally invariant and symmetric indices of diffusion anisotropy. Magn Reson Imaging 1999;17:881–892.
38. Papadakis NG, Xing D, Huang CL, Hall LD, Carpenter TA. A comparative study of acquisition schemes for diffusion tensor imaging using MRI. J Magn Reson 1999;137:67–82.